ACS NANO

Open Access

www.acsnano.org

Role of Chalcogenides in Sensitive Therapeutic Drug Monitoring Using Laser Desorption and Ionization

Sunho Joh,[⊥] Jaekak Yoo,[⊥] Seung Mi Lee, Eunji Lee, Hee-Kyung Na, Jin Gyeong Son, Jeongyong Kim, Mun Seok Jeong, Sang-Guk Lee,* and Tae Geol Lee*

Cite This: *ACS Nano* 2024, 18, 17681−17693

Read Online

ACCESS | Metrics & More | Article Recommendations | Supporting Information

ABSTRACT: **This study investigates the applicability of six transition metal dichalcogenides to efficient therapeutic drug monitoring of ten antiepileptic drugs using laser desorption/ionization-mass spectrometry. We found that molybdenum ditelluride and tungsten ditelluride are suitable for the sensitive quantification of therapeutic drugs. The contribution of tellurium to the enhanced efficiency of laser desorption ionization was validated through theoretical calculations utilizing an integrated model that incorporates transition-metal dichalcogenides and antiepileptic drugs. The results of our theoretical calculations suggest that the relatively low surface electron density for the tellurium-containing transition metal dichalcogenides induces stronger Coulombic interactions, which results in enhanced laser desorption and ionization efficiency. To demonstrate applicability, up to 120 patient samples were analyzed to determine drug concentrations, and the results were compared with those of immunoassay and liquid chromatography−tandem mass spectrometry. Agreements among these methods were statistically evaluated using the Passing−Bablok regression and Bland−Altman analysis. Furthermore, our method has been shown to be applicable to the simultaneous detection and multiplexed quantification of antiepileptic drugs.**

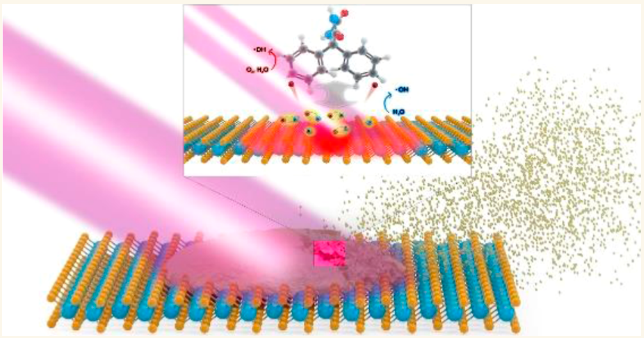

KEYWORDS: *laser desorption ionization, tungsten ditelluride, molybdenum ditelluride, therapeutic drug monitoring, density functional theory, proton affinity, electrostatic repulsion*

INTRODUCTION

Variations in the composition of chalcogenide elements are one of the significant factors leading to the versatile tunability of transition metal dichalcogenides (TMDCs), which critically influences their electronic and thermodynamic properties.[1,2] Specifically, as the chalcogen element changes from S to Te, the number of orbitals increases along with the variation in the electronegativity. This not only plays a significant role in the transition from semiconductive to semimetallic electronic configuration but also influences thermal properties by inducing variations in dipole moments and interatomic interactions.[3,4] These alterations in the electronic and thermodynamic properties consequently lead to distinctive changes in behaviors such as charge transfer and electrocatalysis, thereby impacting the applicability of TMDCs in various fields, including optoelectronics, photocatalytic degradation, electrochemical energy storage, and chemical/biomedical applications.[5−8]

Laser desorption/ionization (LDI)-mass spectrometry (MS) is another field of application with practical significance, where the physicochemical properties of TMDCs can play a critical role. As an analytical tool widely used in pharmaceutical and biomedical analyses, LDI-MS is an easy-to-use technique that provides timeliness, high analytical throughput, and high sensitivity. Since the photocatalytic effect and the photothermal conversion induced by laser irradiation are critical aspects of the LDI process, the overall analytical performance can be strongly influenced by the properties of the ionization assistant reagent, commonly known as the matrix.[9−12] In this

Received: February 21, 2024
Revised: June 7, 2024
Accepted: June 12, 2024
Published: June 26, 2024

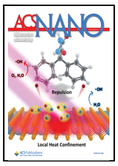

ACS Publications

https://doi.org/10.1021/acsnano.4c02429

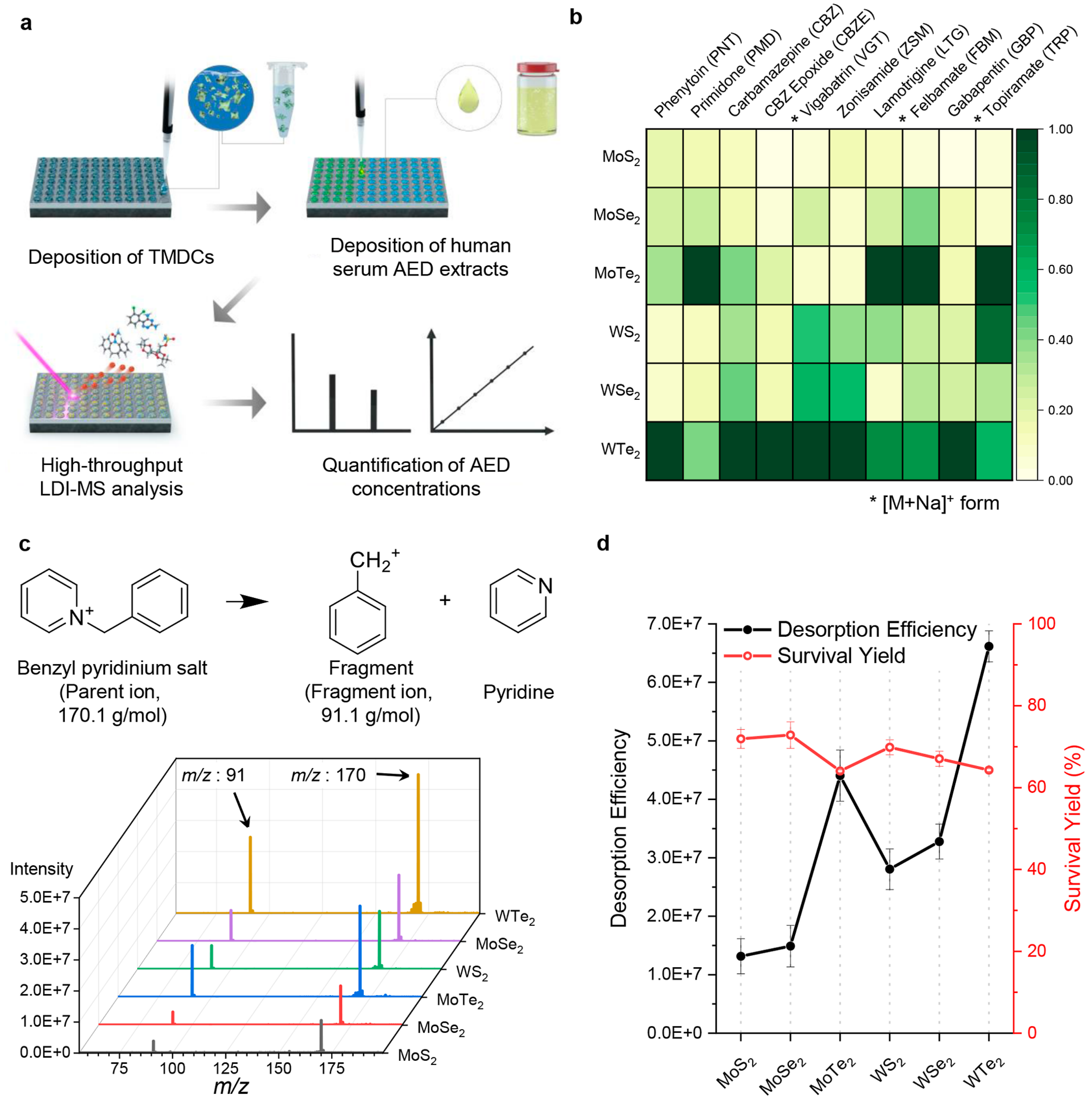

Figure 1. (a) Experimental workflow for the quantitative analysis of AEDs in patient serum samples. (b) Summary of the screening results of TMDCs for the detection of various AEDs. The ion signals obtained by positive mode LDI-MS are normalized to the strongest ion signal for each drug and represented in a heatmap. Asterisks denote AEDs detected in the form of sodium adduct ions. All other AEDs were detected in the $[M + H]^+$ form. (c) Overview of the fragmentation reaction of BP salt and the mass spectra of ions desorbed from each TMDC. $MoTe_2$ and WTe_2 exhibited enhanced signal intensities for both BP and fragment ions. (d) DE and SY for each TMDC.

context, TMDCs such as MoS_2 and WS_2, which are known for their efficiency in photocatalysis and photothermal conversion, have been widely investigated in biomolecule analysis, demonstrating feasibility comparable to that of other extensively studied materials, such as metal nanoparticles and carbon-based nanomaterials.

In particular, our previous work has shown that WS_2 nanosheet-based LDI-MS is an effective tool for the therapeutic drug monitoring (TDM) of immunosuppressive drugs in the blood of organ transplant patients. It has achieved a sensitivity 20 times higher than that of the commonly used organic matrix (e.g., α-cyano-4-hydroxycinnamic acid) while also demonstrating compatibility with liquid chromatography tandem mass spectrometry (LC−MS/MS), a prevalent technique for TDM widely adopted in clinical settings. This demonstrates that TMDCs are promising materials that can significantly enhance the practicality and applicability of LDI-MS to satisfy the various analytical needs of clinical laboratories. Therefore, a comprehensive investigation of the TMDCs from the perspective of LDI-MS is significant,

https://doi.org/10.1021/acsnano.4c02429
ACS Nano 2024, 18, 17681−17693

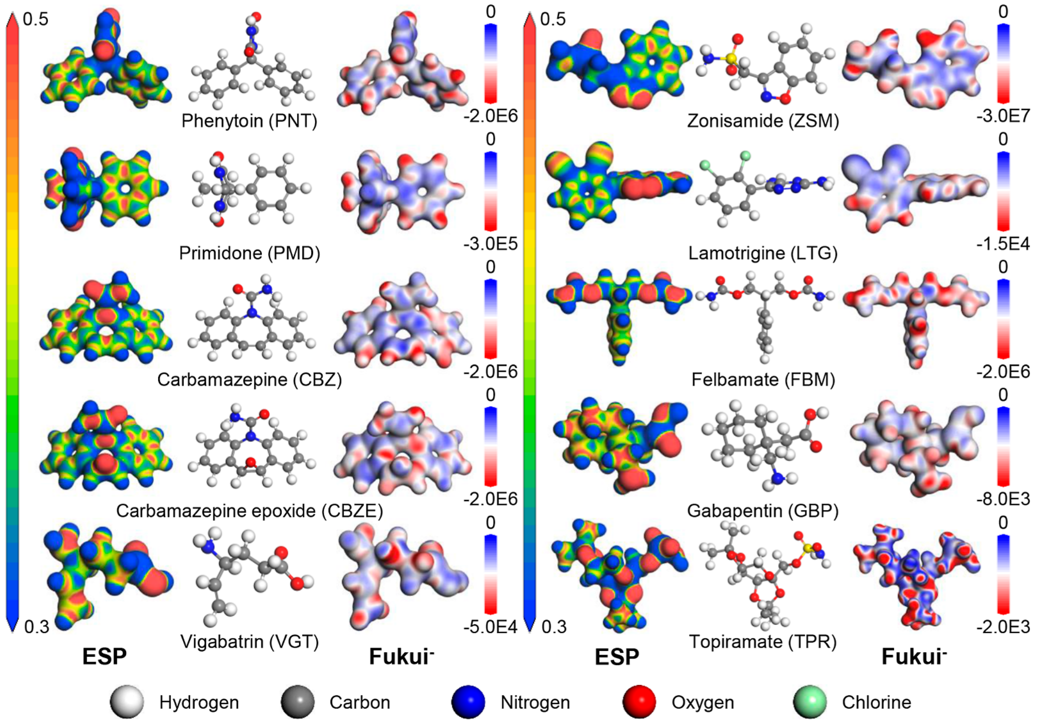

Figure 2. Electrostatic potential (ESP) and Fukui functions (f^-) mapped on the antiepileptic drugs (AEDs). Values in atomic units.

especially considering that it can aid in elucidating the influence of their physicochemical properties on laser-induced ionization. However, this kind of systematic study is relatively scarce, with the notable exception of research on nanoparticles.[13] This makes the study of LDI-MS more reliant on empirical approaches.[14]

Taking these into account, we have investigated the LDI efficiencies of six TMDCs for ten commonly prescribed antiepileptic drugs (AEDs), which are small-molecular-weight medications that require routine TDM. The TMDCs investigated in this study include molybdenum disulfide (MoS_2), molybdenum diselenide ($MoSe_2$), molybdenum ditelluride ($MoTe_2$), tungsten disulfide (WS_2), tungsten diselenide (WSe_2), and tungsten ditelluride (WTe_2). The LDI efficiencies of these TMDCs were evaluated according to the signal intensities of the AEDs and the desorption efficiency (DE) and survival yield (SY) of the benzylpyridinium (BP) salt. On the basis of the evaluation results, it was identified that $MoTe_2$ and WTe_2 have a pronounced LDI efficiency, indicating that they are suitable materials for the sensitive detection of therapeutic drugs. Subsequently, density functional theory (DFT) calculations were employed to examine the influence of chalcogenides on LDI efficiency. Specifically, we present an integrated theoretical calculation model that can adaptively reflect the experimental environments to better describe the thermodynamic interactions within the system. In details, unlike approaches that rely on conventional chemical properties (e.g., charge density and reaction energy), a systematic study was conducted by establishing up to 60 integrated systems that incorporate the TMDCs and AED molecules adsorbed onto their surfaces, which allows for the calculation of proton affinities.

Finally, to demonstrate the effectiveness of LDI-MS utilizing $MoTe_2$ and WTe_2 in clinical drug monitoring, we analyzed up to 120 serum samples from patients treated with commonly prescribed AEDs, namely, carbamazepine (CBZ), lamotrigine (LTG), and topiramate (TPR), and determined their concentrations (Figure 1a). The results obtained by LDI-MS were compared with those of the immunoassay and LC−MS/MS, and the agreements were evaluated using the Passing−Bablok regression and Bland−Altman analysis. The applicability of our method to the multiplexed quantification of the three AEDs was also examined.

RESULTS AND DISCUSSION

Screening of TMDCs for the LDI-MS Analysis of AEDs.

To select the optimal materials for the TDM of AEDs, we investigated the LDI efficiencies of six extensively studied TMDCs, namely, MoX_2 (X = S, Se, and Te) and WX_2.[15−17] To the best of our knowledge, aside from MoS_2 and WS_2, the LDI efficiencies of these materials have not been extensively explored.[18−20] For a systematic screening of various AEDs, representative drugs were selected based on the AED classification outlined in the work of Rho and White.[21] Specifically, the first-generation AEDs include phenytoin (PNT) and primidone (PMD); the second-generation AEDs comprise CBZ and CBZ epoxide; and the third-generation AEDs consist of zonisamide (ZSM), LTG, gabapentin (GBP), and TPR.

Figure 1b summarizes the screening results of the TMDCs in the form of a heatmap (raw data are shown in Table S1). Overall, all TMDC materials investigated in this study, which contain transition metal atoms of Mo and W, were able to assist in the ionization of up to ten commonly prescribed AEDs. Notably, among the six TMDC materials, $MoTe_2$ and WTe_2 tend to have an enhanced LDI efficiency, as indicated by the higher total ion counts. For example, the experimental results indicated that WTe_2 can effectively assist in the ionization of the earlier generations of AEDs such as PNT, CBZ, and CBZ epoxide, while $MoTe_2$ is more suitable for assisting the ionization of the newer-generation AEDs

https://doi.org/10.1021/acsnano.4c02429

Table 1. Reaction and Activation Energy of Non-Assisted Protonation of AEDs

energy (eV)	PNT	PMD	CBZ	CBZE	VGT	ZSM	LTG	FBM	GBP	TPR
reaction energy	4.99	4.54	4.08	4.25	4.88	3.81	4.72	5.13	4.98	5.18
activation energy	6.88	6.89	6.76	6.85	6.90	7.24	6.84	6.90	6.84	7.02

including LTG and TPR. In addition, the LDI efficiency tends to increase from S to Te within the same transition metal element (i.e., Mo and W). For instance, compared to MoS_2 and $MoSe_2$, $MoTe_2$ demonstrated greater efficiency in assisting the ionization of all AEDs with the exception of vigabatrin (VGT) and ZSM. A similar trend was observed for WTe_2 with the exception of TPR, suggesting that the presence of tellurium is one of the significant factors that leads to enhanced LDI efficiency.

These observations were further examined using BP salt, a thermometer molecule commonly employed to study the photoinduced desorption process occurring at the surface during laser irradiation.[22,23] Since BP has an intrinsic cation in its structure, the desorption process facilitated by factors such as photothermal conversion can be studied exclusively by calculating the DE and the SY, where DE = $\text{intensity}_{(m/z\sim91)}$ + $\text{intensity}_{(m/z\sim170)}$ and SY = $\text{intensity}_{(m/z\sim170)}/(\text{intensity}_{(m/z\sim91)} + \text{intensity}_{(m/z\sim170)})$. As shown in Figure 1c,d, $MoTe_2$ and WTe_2 exhibited an enhanced DE by a factor of approximately ∼4 and ∼7, respectively, compared to their disulfide counterparts (i.e., MoS_2 and WS_2), while the SY of all TMDCs was within the range of 64−72%. This result implies that the extent of desorption upon laser irradiation is one of the key factors that determines the LDI efficiency of various TMDC materials. To further elucidate these intriguing observations, we employed DFT, which is a widely used method to describe electronic structures.

In-Depth Study of LDI Efficiencies of TMDCs. *Ab Initio Study of the Chemical Reactivity of AEDs.* Quantum mechanical simulations can facilitate the understanding of various physical properties by modeling the actual situation, rather than relying on empirical methods.[24] Specifically, first-principles calculations using DFT enable the estimation of electronic interactions occurring at the atomic scale.[25−27] For example, Fukui functions can be used to identify the electrophilic and nucleophilic sites as well as to visualize the electrostatic potential (ESP) of molecular systems by providing information on charge distribution.[28] In addition, the activation energies for chemical reactions such as protonation can be estimated, which can provide valuable chemical information to the studies of mass spectrometry.[29,30]

In this context, we adopted DFT calculations to identify the governing physicochemical parameters related to the ionization process. Figure 2 represents the results of the calculations for the ESP and Fukui functions (f^-) of the AEDs used in this study. For ESPs, all AEDs were within atomic unit values ranging from 0.3 to 0.5, a range common for molecules with atoms of high electronegativity (e.g., oxygen and nitrogen) or alternating sp^2-hybridized carbon bonds with high local charge density (e.g., aromatic rings). Notably, TPR and felbamate (FBM) had electron densities localized to the oxygen-bearing bonds, which can be attributed to the high electronegativity of the O atoms present in the ether groups. However, the atomic unit values of these drugs were also within the 0.3−0.5 range, similar to those of other AEDs with more evenly distributed charge density. This indicated that no AED is preferentially more accessible to positive charges such as proton or alkali metal cations, which are adduct ions commonly observed in mass spectra (e.g., $[M + Na]^+$ and $[M + K]^+$). Therefore, this result suggests that while ESP can partially estimate a more reactive site of a molecule, it alone cannot fully explain the reactivity of AEDs.

For a more straightforward representation of the reactivity of various AEDs, f^- was calculated using the finite-difference approximation, as defined by the following equation.

$$f^-(r) = \frac{1}{\Delta N}(\rho_N(r) - \rho_{N-\Delta}(r)) \tag{1}$$

As illustrated in Figure 2, f^- generally exhibited a trend similar to that of the ESP map, showing relatively high reactivity for atoms with high electronegativity such as oxygen and nitrogen. Upon detailed inspection, however, it was observed that several AEDs exhibit pronounced reactivity when considering the absolute values of f^- for each drug. According to eq 1, f^- is a function of changes in charge densities induced by the loss of an electron. Therefore, a higher absolute value for f^- indicates that the changes in charge densities have been induced to a greater extent, which can be translated into a higher chemical reactivity.[31] Hence, by reflecting the absolute value of f^-, the reactivities of each AED can be estimated in the order ZSM > PNT ∼ PMD ∼ CBZ ∼ CBZE ∼ FBM > PMD > VGT ∼ LTG > GBP ∼ TPR. A similar trend was observed with f^+, suggesting that the AEDs identified as chemically reactive based on the absolute values of f are also prone to nucleophilic attack, as shown in Figure S1 (Supporting Information).

To further analyze the chemical reactivities of the AEDs, we calculated the activation energies for the protonation reaction as this is one of the most widely adopted DFT-based approaches for studying the ionization process in mass spectrometry.[29,32] The activation energies for protonation can describe the ionization process more comprehensively as the atomic interactions between drugs and a proton are taken into account, whereas ESP, f^-, and f^+ are more suitable for the identification of the intrinsic reactivity of a molecule. Since desorption is one of the key features of the LDI process, the H_2O molecule (i.e., proton source) was positioned approximately ∼12 Å away from the AED to ensure that interactions between the OH^- molecule and the protonated AED are negligible (Figure S2, Supporting Information). The calculated reaction and activation energies for protonation are summarized in Table 1. Generally, the reaction energies of the AEDs showed a trend similar to their intrinsic reactivity as estimated by f^-, with ZSM exhibiting the lowest reaction energy and TPR exhibiting the highest reaction energy.

However, the activation energies showed a different trend. Specifically, our calculations showed that the activation energies are significantly higher than the reaction energies by ranging from 6.76 to 7.24 eV. This indicates that protonation of AED is hardly a spontaneous reaction, where the activation energy and the external energy to overcome the barrier play a critical role. Furthermore, the correlation between the tendencies of the activation and reaction energies appears to be weak. For example, ZSM had to overcome the highest activation barrier to be protonated, although it had the lowest

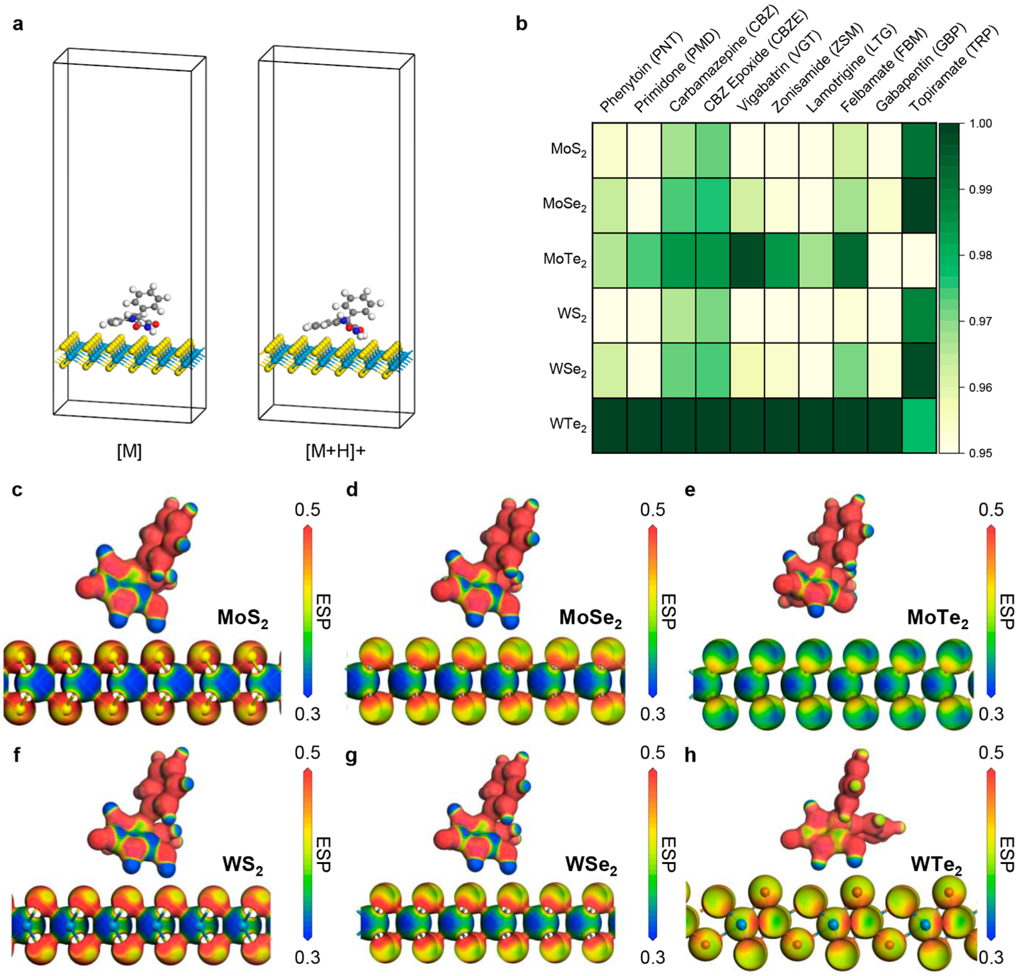

Figure 3. Analysis of laser desorption and ionization (LDI) efficiencies. (a) Ball-and-stick model of the integrated transition metal dichalcogenide-antiepileptic drug (TMDC-AED) system. The efficiency of the LDI process was determined by calculating the difference in enthalpy between the two states of the system: the protonated state, denoted as $[M + H]^+$, and the neutral state, represented as $[M]$. (b) The heatmap shows the calculation results of 60 TMDC-AED systems. Consistent with the previous experimental results, the tellurium-containing TMDCs have the highest LDI efficiency. (c−h) Representative ESP map of the 60 TMDC-AED systems, showing that the tellurium-containing TMDCs have a relatively low surface charge density.

reaction energy. Cumulatively, these results suggest that the variance in LDI efficiency cannot be fully explained by intrinsic molecular properties alone, such as charge density or reaction energy.

Physicochemical Parameters for Determination of the LDI Efficiency of TMDC-AEDs. One of the practical methods to estimate the ionization efficiency of a molecule is to determine the proton affinity (PA).[33,34] As a chemical parameter correlative to ionization efficiency, many studies have reported that analytes with a high PA tend to be more efficiently ionized, resulting in higher mass spectrometry signals.[35−37] As demonstrated in the work of Grechnikov et al., PA can be thermodynamically derived from the change in enthalpy for a protonation reaction, as shown in eq 2.[33] This approach allows for a more comprehensive estimation of ionization efficiency as it considers the change in internal energy of a system during protonation rather than solely relying on the intrinsic properties of a molecule.

$$\mathrm{PA} = \Delta H^\circ_{\mathrm{A}} + \Delta H^\circ_{\mathrm{H+}} - \Delta H^\circ_{\mathrm{AH+}} \tag{2}$$

Therefore, we postulated that an in-depth investigation of the role of TMDCs could be achieved by considering the presence of the TMDC layer when estimating the enthalpy (i.e., PA). To this end, we have formulated a model in which the AED and TMDC layers are incorporated within a single system (Figure 3a). Using this integrated system, the PAs of each AED in relation to different types of TMDCs were determined by theoretical calculations. Figure 3b represents the estimated ionization efficiencies of AEDs in the form of a heatmap. Interestingly, all AEDs with WTe_2 had the highest ionization efficiencies except TPR, suggesting that WTe_2 is the most suitable ionization assistant reagent for the analysis of AEDs. The AEDs with $MoTe_2$ generally exhibited a higher ionization efficiency among the MoX_2 TMDCs with the exception of TPR, while several drugs such as VGT and FBM showed efficiencies comparable to those with WTe_2. This result suggests that WTe_2 and $MoTe_2$ can enhance the ionization sensitivity of AEDs, corroborating the experimental results shown in Figure 1b.

As one of the critical factors determining LDI efficiency, which is associated with enhanced intensity of the MS signal, thermal-driven desorption has gained significant attention.[38−42] In detail, ionization assistant reagents with low thermal conductivity can induce local heat confinement upon laser irradiation more efficiently, leading to a higher ion-desorption efficiency.[13,14,43,44] Recently, Cheng and Ng showed that the desorption process can also be highly influenced by the extent of hole generation.[45,46] Specifically, desorption can be facilitated by electrostatic repulsion between positively charged analytes and holes generated on the substrate surface upon laser irradiation (i.e., charge-driven desorption).[45]

As can be seen from the results of the optical spectroscopic analyses in Figure S3 (Supporting Information), a blue shift of 1.4 cm^{-1} in the A_1' Raman mode was observed on the surface of MoS_2 deposited with AED. The photoluminescence (PL) and time-resolved PL spectra also indicated that a blue shift is present with an increase in PL and lifetime. These results cumulatively indicate that the TMDC surface is p-doped to generate holes with partial positive charges. This suggests that the difference in hole generation efficiency can be one of the significant factors contributing to the differences in LDI efficiencies for various TMDCs (Figures 1b and 3b).

To better understand this behavior, the ESP maps for the protonated systems, which include the TMDC and the protonated structure of the AED, were calculated (Figure 3c−h). Interestingly, the surfaces of $MoTe_2$ and WTe_2 tend to be more electron-deficient (i.e., more positively charged) compared with other TMDCs with disulfide and diselenide, suggesting that AED ions may undergo stronger Coulomb repulsion, leading to more efficient desorption. For further investigation, the distance between the protonated AED and the TMDC was calculated as a measure of the extent of the repulsive interaction (Figure S4, Supporting Information). Among the 10 AEDs, $MoTe_2$ exhibited the maximum interaction distance, with seven drugs within the MoX_2 TMDC group. Similarly, WTe_2 showed the maximum, with eight drugs among the WX_2 TMDCs. This indicates that $MoTe_2$ and WTe_2 are more favorable for facilitating the desorption of the ionized analytes.

These observations coincide with the experimental results in Figure 1c,d, which show that $MoTe_2$ and WTe_2 had the highest signal intensities and DE values for the BP salt. Considering that the intrinsic positive charge in the structure of BP makes its ionization efficiency relatively less crucial, the enhanced signal intensity and DE of BP provided by $MoTe_2$ and WTe_2 should be attributed to the facilitation of charge-driven desorption. In addition, WTe_2 has the lowest thermal conductivity among MoX_2 and WX_2 TMDCs, while $MoTe_2$ has the lowest thermal conductivity among MoX_2 TMDCs according to the literature.[47,48] Consequently, these properties further enhance the favorability of the thermally driven desorption process.

Furthermore, the generation of holes can lead to the transfer of excited electrons to surface adsorbents (e.g., residual H_2O, O_2, and AED molecules) or to their thermal dissipation.[9−11] These can lead to LDI-favorable processes other than Coulomb repulsion such as the generation of reactive hydroxyl radicals and local heat confinement. Therefore, we attribute the enhanced LDI efficiency of $MoTe_2$ and WTe_2 to the synergistic contribution of their electronic and thermal properties, which facilitates both thermal and charge-driven desorption (Scheme 1).

Application of $MoTe_2$/WTe_2 Mixture-Assisted LDI-MS in Therapeutic Drug Monitoring. *Quantitative Analysis of AEDs.* The applicability of $MoTe_2$ and WTe_2 to TDM was further examined by analyzing the AEDs in blank human serum. Based on the experimental results in Figure 1, a mixture of $MoTe_2$ and WTe_2 was used to facilitate the quantification of CBZ, LTG, and TPR. To compensate for variations in extraction efficiency and improve analytical precision, stable isotope-labeled internal standards were introduced, a technique commonly used in quantitative LC−MS/MS analysis (Figure S5, Supporting Information). Since the internal standards labeled with isotopes share similar physicochemical properties with the original target drugs, they can be extracted and ionized to a similar extent, while they can be distinguished in MS spectra by the difference in m/z values. For these reasons, the peak intensities of the internal standards were used to normalize the MS signals obtained from the AEDs.

Scheme 1. Schematic Representation of the Laser Desorption Ionization Process Assisted by Transition Metal Dichalcogenides[a]

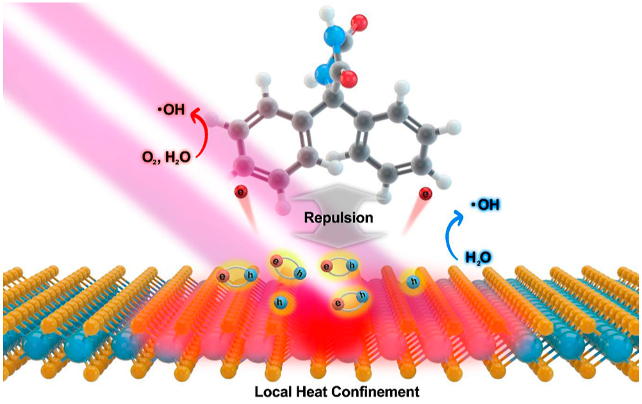

[a]Electron−hole pairs generated by absorbing laser energy synergistically contribute to the ionization of AEDs. Local heat confinement and electrostatic repulsion between the holes and the positively charged AEDs facilitate the thermal- and charge-driven desorption processes, respectively.

To verify the applicability of the $MoTe_2$/WTe_2 mixture, blank human serum was spiked with AEDs and their corresponding internal standards (1 μL, 10 μg/mL concentration) mixture and was extracted via solid-phase extraction. Subsequently, the human serum AED extracts were pipetted on the surface of the predeposited $MoTe_2$/WTe_2 mixture and analyzed via LDI-MS after immediate drying under ambient conditions. The mass spectra of CBZ, LTG, and TPR showed that the $MoTe_2$/WTe_2 mixture assisted the simultaneous LDI of both AED and internal standards (Figure 4a−c). For the CBZ extract, the peaks of CBZ and CBZ-$^{13}C^{6}$ were detected at the m/z of 259 and 265 corresponding to their $[M + Na]^+$ forms, respectively. For the LTG and TPR extracts, the AED peaks were detected at the m/z of 278 and 362, while their internal standard peaks were detected at the m/z of 282 and 374, respectively. These results demonstrate that the $MoTe_2$/WTe_2 mixture effectively assists the LDI process of AEDs extracted from human sera while minimizing background interference in the low m/z region (Figure S6, Supporting Information), which is an essential factor for the analysis of low-molecular-weight biomolecules or pharmaceutical drugs.

For quantification, each human serum AED extract within the clinically significant concentration range (1−100 μg/mL) was measured three times. The intensities of the AED peaks were normalized by those of the corresponding internal standards to obtain the peak area ratio. The calibration curves

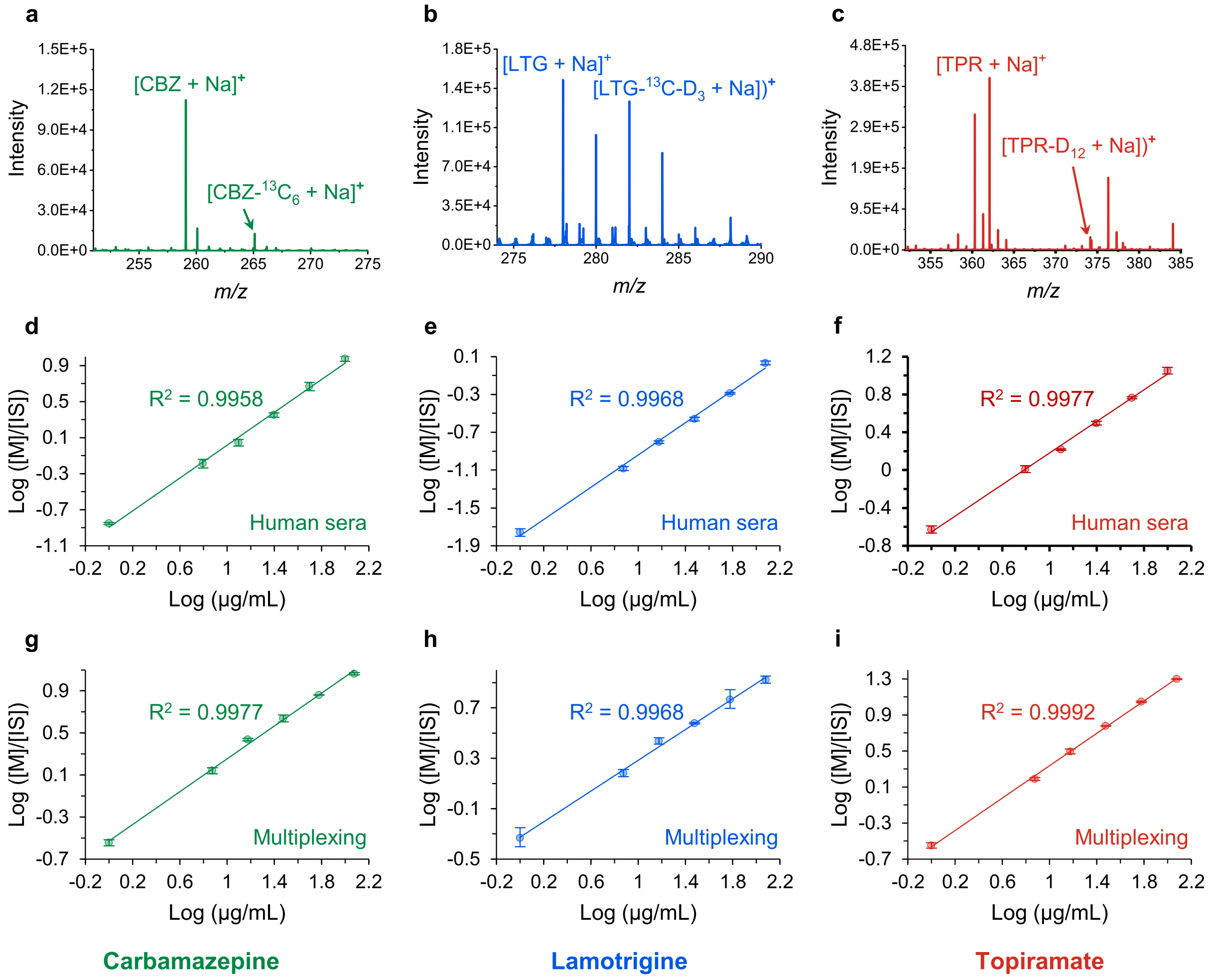

Figure 4. (a−c) Mass spectra of human serum AED extracts obtained using $MoTe_2/WTe_2$ mixture-assisted LDI-MS at a concentration of 10 μg/mL. (d−f) Calibration curves constructed from LDI-MS analysis of human serum extracts with varying concentrations of spiked-in AEDs, within a 1−100 μg/mL concentration range. (g−i) Calibration curves obtained through multiplexed quantification of AED mixtures. Error bars represent the standard deviation ($n = 3$).

Table 2. Recovery and Precision Test for (a) CBZ, (b) LTG, and (c) TPR Spiked in Blank Human Serum[a]

expected concentration (μg/mL)	meas. one (μg/mL)	meas. two (μg/mL)	meas. three (μg/mL)	mean (μg/mL)	mean recovery (%)	coeff. of var. (%)
			(a)			
12.5	11.12	11.77	12.56	11.81	94.51	6.01
6.25	6.25	5.97	5.91	6.05	96.73	3.03
1	1.29	1.35	1.37	1.34	134.11	2.91
			(b)			
15	17.15	16.33	16.10	16.53	110.19	3.35
7.5	7.72	8.56	7.92	8.07	107.57	5.43
1	0.46	0.81	0.72	0.66	66.34	27.46
			(c)			
12.5	12.69	12.30	12.42	12.47	99.74	1.61
6.25	6.69	6.06	5.91	6.22	99.56	6.65
1	1.25	0.88	0.99	1.04	104.20	18.50

[a] Clinically significant concentrations were selected based on the therapeutic concentration ranges of patients treated with AEDs.

were constructed based on the peak area ratios of the six-level calibrators, and their linearities were determined by calculating the coefficient of determination (R^2) (Figure 4d−f). All three AEDs tested in this study, namely, CBZ, LTG, and TPR, demonstrated a linear correlation with R^2 values greater than 0.99 within the therapeutic concentration range, specifically 0.9958 for CBZ, 0.9968 for LTG, and 0.9977 for TPR. These results indicate that the ion signals obtained by $MoTe_2/WTe_2$ mixture-assisted LDI-MS can yield reproducible and linear calibration curves suitable for the quantification of AEDs in human serum. The reliability of our method was further validated by examining the percent recovery and precision. The amount of drugs measured in the AED-spiked human sera

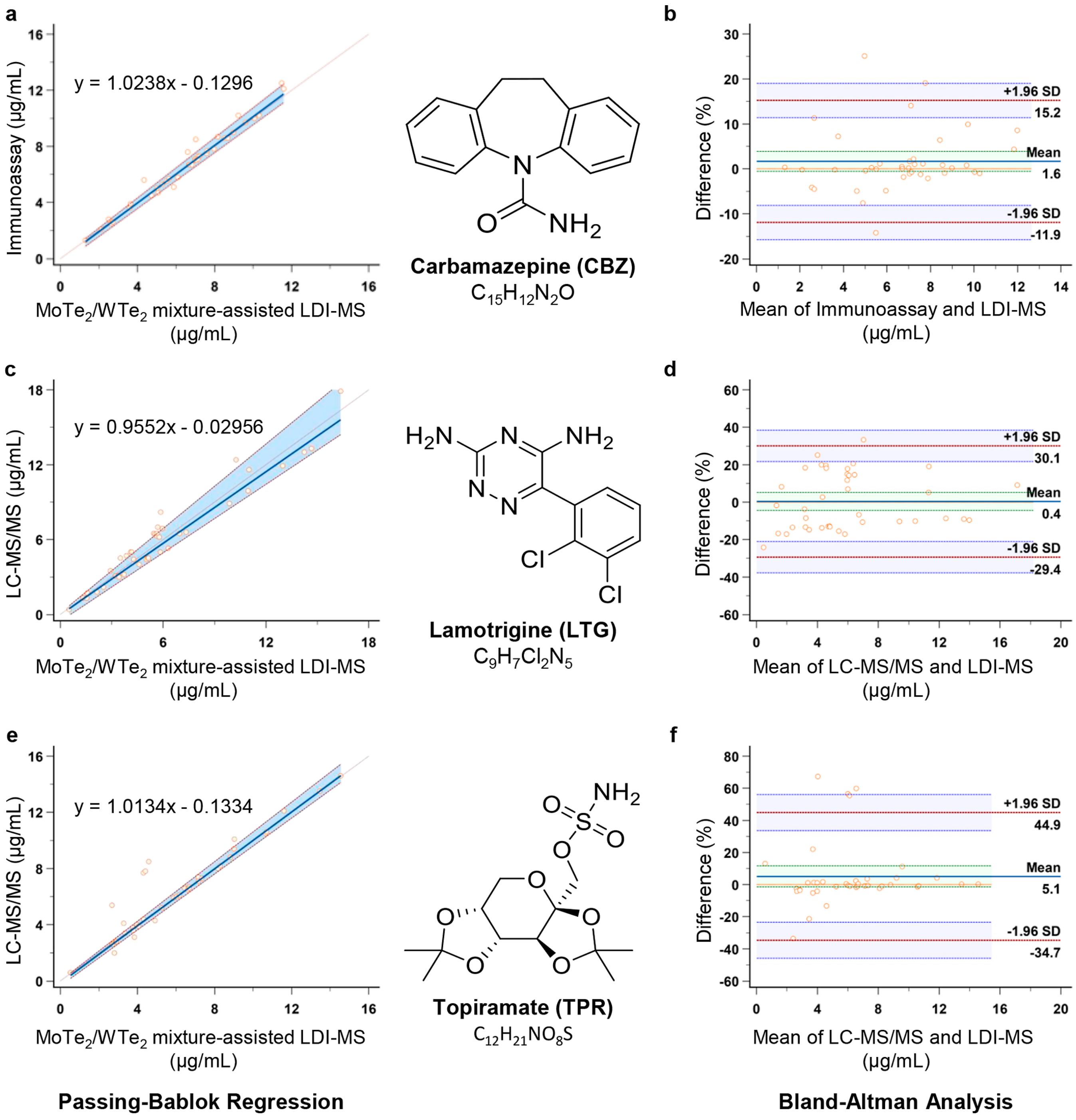

Figure 5. Passing−Bablok regression (left) and Bland−Altman analysis (right) for the quantification results of carbamazepine (a,b), lamotrigine (c,d), and topiramate (e,f). For carbamazepine, the LDI-MS results were compared with those from immunoassay. For lamotrigine and topiramate, the LDI-MS results were compared with those from LC−MS/MS. For each drug, 40 patient serum samples were analyzed.

and their corresponding percentages of recovery and coefficients of variation (CV) are shown in Table 2.

Notably, approximately 30% of patients treated with AEDs undergo polytherapy, which involves the concurrent administration of more than two types of drugs.[49−51] Given that several studies have demonstrated that MALDI-MS is capable of simultaneous quantification of analytes such as protein biomarkers or neurotoxins,[52−55] our method was further examined for multiplexed quantitative analysis of three types of AEDs, namely, CBZ, LTG, and TPR. As demonstrated in Figure S7 (Supporting Information), the major AED and internal standard-related peaks were detected in their sodiated form and were clearly distinguishable by their differences in the m/z values, which was similar to the results shown in Figure 4a−c. For quantification, a mixture of AEDs containing CBZ, LTG, and TPR was serially diluted within the clinically significant range (1−100 μg/mL), and a mixture of their corresponding internal standards was added separately for normalization. As shown in Figure 4g−i, the calibration curves of all three AEDs had R^2 values greater than 0.99 (i.e., R^2

values of 0.9977, 0.9968, and 0.9992 for CBZ, LTG, and TPR, respectively) within the therapeutic range. This suggests that our method can be further applied to the TDM of medications that require multiplexed quantification, such as anticancer drugs, antiviral drugs, and antibiotics.[56−58]

Interassay Assessment of LDI-MS with Immunoassay and LC−MS/MS. The analytical performance of $MoTe_2/WTe_2$ mixture-assisted LDI-MS for the TDM of AEDs was further examined by comparing its results with those of techniques commonly used in real-world clinical settings. To date, approximately 29 AEDs have been widely prescribed in the real-world clinical setting, while routine TDM of these drugs is commonly performed using analytical techniques such as immunoassays and LC−MS/MS.[59−61] In particular, many early-generation AEDs, such as CBZ, rely mainly on immunoassay techniques, while newer-generation AEDs, including LTG and TPR, prefer LC−MS/MS methods.[62,63]

Therefore, human serum samples from 120 patients treated with CBZ (40 patients), LTG (40 patients), and TPR (40 patients) were analyzed using the LDI-MS method, and drug concentrations were determined. For CBZ, the results were compared with those obtained by immunoassay, while the results of LTG and TPR were compared with those obtained by LC−MS/MS. To statistically assess the agreement between the LDI-MS and comparative methods, Passing−Bablok regression and Bland−Altman analysis were used (Figure 5). The results of the Passing−Bablok regression showed that there is no statistically significant bias for the LDI-MS method compared to the immunoassay and LC−MS/MS methods (Figure 5a,c,e). Specifically, the 95% confidence interval (CI) of the slopes of CBZ (0.9955−1.0713), LTG (0.9138−1.1284), and TPR (0.9948−1.0598) encompassed 1, indicating that there is no proportional bias in the LDI-MS results. The 95% CI of the intercepts of CBZ (−0.4177 to 0.03536), LTG (−0.5441 to 0.1179), and TPR (−0.3482 to 0.01143) included 0 respectively, demonstrating the absence of constant bias.

The results of the Bland−Altman analysis showed that the mean difference of the results of CBZ was 1.64%, while those of LTG and TPR were 0.37 and 5.08%, respectively (Figure 5b,d,f). Although a small positive bias was observed for the TPR samples, the analysis results of most samples were within the acceptable limit of ±1.96 standard deviation (SD) for the three AEDs, indicating that the LDI-MS results corresponded well to those of the immunoassay and LC−MS/MS.[64] Furthermore, the 95% CI of the mean difference for CBZ (−0.5717 to 3.8564%), LTG (−4.4843 to 5.2186%), and TPR (−1.4115 to 11.5680%) included 0, showing that there are no significant statistical differences between LDI-MS and the comparative methods.

Overall, the results of the Passing−Bablok regression and Bland−Altman analysis indicated that the $MoTe_2/WTe_2$ mixture-assisted LDI-MS is suitable as an alternative analysis technique for the TDM of AEDs in human serum. Given that LDI-MS has advantageous features such as high analytical throughput, short turnaround time, and cost-effectiveness, our method is expected to satisfy the demands of clinical laboratory settings effectively. A comparison between the measured concentration values (i.e., immunoassay, and LC−MS/MS) is shown in Figures S8−S10.

CONCLUSIONS

We have experimentally screened for the TMDCs suitable for the efficient TDM of AEDs using LDI-MS. The tellurium-based TMDCs exhibited enhanced ion counts, which can be approximately 10−100 times higher, allowing for the sensitive quantification of therapeutic drugs in human serum. Additionally, the results of the Passing−Bablok regression and the Bland−Altman analysis indicated that LDI-MS is compatible with immunoassays and LC−MS/MS, the mainstay techniques for TDM in clinical settings. Furthermore, our theoretical calculations showed that our systematic approach can better explain the LDI process compared to conventional methods (e.g., charge density and reaction energy) by adequately describing the surficial interactions occurring at the atomic scale. This suggests that our comprehensive methodology can be further applied to the screening and selection of candidate materials for LDI-MS, while it can also serve as an effective method for validating the experimental results. We anticipate that our study will provide a foundation for understanding the interactive nature of TMDCs and therapeutic drugs. In addition, our work is expected to be beneficial for researchers investigating the fundamental nature and versatile applications of various TMDC materials.

EXPERIMENTAL SECTION

Materials. The chemical vapor transport (CVT)-grown 2H−MoS_2, 2H−$MoSe_2$, 2H−WS_2, and 2H−WSe_2 were purchased from 2D Semiconductors, and 2H−$MoTe_2$ and Td−WTe_2 were purchased from Ossila. The solutions of $MoTe_2$ and $WTe2_2$ flakes dispersed in isopropyl alcohol, prepared by ultrasonication treatment of the crystals, were purchased from 2D Semiconductors. The Raman scattering spectra of TMDCs are shown in Figure S11 (Supporting Information). PNT, PMD, CBZ, carbamazepine epoxide (CBZE), VGT, ZSM, LTG, FBM, GBP, TPR, CBZ−$^{13}C_6$, LTG−^{13}C, D_3, TPR−D_{12}, methanol, and human serum were purchased from Sigma-Aldrich and were used without purification. Patient samples (CBZ, LTG, and TPR) were received from Severance Hospital. The experiments were approved by the Institutional Review Board of Severance Hospital (IRB no. 4-2019-0944).

Solid-Phase Extraction. For LDI-MS analyses, extraction of the AEDs-spiked human serum and the patient samples were performed via solid-phase extraction according to the method reported by Kuchekar et al. with appropriate modification.[65] In brief, 15 μL of the AED and internal standards mixture were added to 95 μL of blank human serum and were mildly vortex. Subsequently, 775 μL of 0.05 M NaOH (aq) was added. The Oasis HLP (Waters, 1 mL/30 mg) cartridges were conditioned and equilibrated with 1 mL of MeOH and deionized water. Upon the loading of the samples, the cartridges were washed with 1 mL of deionized water and 1 mL of 5% MeOH. After washing, the samples were eluted with 1 mL of MeOH. For clinical samples, 15 μL of a mixture of MeOH and internal standards were added in the place of AEDs and were extracted via an identical process.

Protein Precipitation. For LC−MS/MS analyses of LTG and TPR, the AEDs spiked human sera, and the patient samples were pretreated by using the protein precipitation method. In brief, 10 μL of the patient samples, each treated with LTG and TPR, was added with 5 μL of their corresponding internal standards. Upon the addition of 295 μL of 100% MeOH, the mixtures were vortexed for 60 s followed by centrifugation at 12,700 rpm for 10 min. After centrifugation, 50 μL of the organic layer was isolated and was added with 150 μL of 0.1 formic acid in distilled water. Subsequently, the mixtures were vortexed for 60 s, and 2 μL of the aliquots was injected into the Sciex triple quad 4500 MD instrument for LC−MS/MS analysis.

Mass Spectrometry Analysis. All LDI-MS analyses were performed in positive polarity mode using a Synapt G2 mass spectrometer (Waters, USA) equipped with a 1 kHz Nd/YAG laser (355 nm wavelength) for MALDI measurement. An auto quadrupole profile was used, while the trap collision energy and transfer collision energy were set to 4.0 and 2.0 V, respectively, for all measurements. For the precise deposition of TMDCs and AEDs, disposable hydrophobic *μ*focus MALDI plates (Asta Inc., Korea) were used, which can facilitate quantitative analysis by improving spot homogeneity and signal reproducibility. In brief, the *μ*focus was attached on the surface of the Waters MALDI target plate, and the solution of dispersed TMDCs (1 *μ*L) was spotted by manual pipetting. After drying under ambient conditions, the AED samples were deposited to be analyzed by LDI-MS. For the screening of TMDCs, CVT-grown TMDCs dispersed in isopropanol (1 mg/mL) were used, while the concentration of all AEDs was 10 *μ*g/mL. For quantitative analysis of AEDs in the human serum samples, a mixture of the $MoTe_2$ and $WTe2_2$ flake solution dispersed in isopropanol was used. For all LDI-MS measurements, a spiral laser pattern with a 3 mm/min line speed was used, and up to 300 shots from the varying positions on the spots of the $MoTe_2$/WTe_2 mixture were taken and averaged to improve the signal uniformity.

For LC−MS/MS analyses, a Sciex triple quad 4500 MD mass spectrometer (Sciex, USA) coupled with HPLC was used in positive polarity mode. The LTG and TPR samples were separated with a constant flow rate of 400 *μ*L/min by using the following binary gradient of mobile phase A (distilled water with 2 mM ammonium acetate and 0.1% formic acid) and B (methanol with 2 mM ammonium acetate and 0.1% formic acid): 10−70% of mobile phase B for 1.5 min, 70−90% for 1.5 min, 90% for 1 min, and 10% for 2.4 min. HPLC−MS/MS was performed in selective reaction monitoring (SRM) analysis mode, and the retention times for LTG ($[M + H]^+$, 256 → 109 *m*/*z*) and TPR ($[M + NH_4]^+$, 357 → 264 *m*/*z*) were 2.71 and 3.06 min, respectively. For the internal standards, the retention time of $^{13}C_3$−LTG ($[M + H]^+$, 259 → 145 *m*/*z*) was 2.71 min and that of d_{12}-TPR ($[M + NH_4]^+$, 369 → 288 *m*/*z*) was 3.04 min.

Immunoassay Analysis for CBZ Quantification. The CBZ patient samples were analyzed according to the manufacturer's instructions for the ONLINE TDM carbamazepine (CARB2) kit for the Cobas C702 analyzer (Roche Diagnostics GmbH, Germany), which measures the kinetic interaction of microparticles in solution (KIMS).

Theoretical Calculation for Properties of Various AEDs. The fundamental properties of various AEDs were calculated using the DMOL3 code, as implemented in the BIOVIA Materials Studio platform.[66] During the calculation, the 10 AEDs were modeled and geometry optimized with a B3LYP hybrid functional.[67] The double-numerical atomic orbitals with polarization were chosen for the basis sets, and all electrons with a relativistic effect were considered for the core parts. Geometries were optimized until the maximum force on each atom was less than 0.002 Ha/Å and the total energy change was less than 10^{-5} Ha. The ESP of the total electron density and the contributions from each atomic orbital on each atom were calculated using the Mulliken analysis method. The electro/nucleophilic sites of AEDs were investigated using the Fukui functions,[68,69] and the activation energy of the protonation reaction was calculated by transition state search using the LST/Optimization synchronous transit protocol[70] with the RMS tolerance of 0.002 Ha/Å.

Afterward, the integrated systems of TMDC-AED were modeled to fully reflect the experimental conditions. The exchange−correlation functionals with generalized gradient approximation[71] and the *k*-points samplings by the Monkhorst−Pack grid with an equidistance of 0.02 $Å^{-1}$ were chosen. The TMDCs were modeled and optimized using the 2H phase of MoS_2, $MoSe_2$, $MoTe_2$, WS_2, and WSe_2 and the 1T phase of WTe_2. We applied 60 Å of vacuum slab to sufficiently isolate the TMDC-AED systems. The lattice constants of bulk TMDCs by DFT calculations for comparison were as follows: $a = b = 3.207$ Å for MoS_2, $a = b = 3.326$ Å for $MoSe_2$, $a = b = 3.536$ Å for $MoTe_2$, $a = b = 3.178$ Å for WS_2, $a = b = 3.299$ Å for WSe_2, and $a = 6.271$ Å, $b = 3.477$ Å for WTe_2. The lattice constants of optimized bulk TMDCs using calculational parameters listed above were as follows: $a = b = 3.18$ Å for MoS_2, $a = b = 3.32$ Å for $MoSe_2$, $a = b = 3.549$ Å for $MoTe_2$, $a = b = 3.18$ Å for WS_2, $a = b = 3.32$ Å for WSe_2, and $a = 6.311$ Å, $b = 3.503$ Å for WTe_2.[72−75] After optimizing the geometry of the TMDCs, we constructed a TMDC supercell that ensures a minimum distance of 10 Å between the AED molecules to avoid interaction effects and thus effectively model the TMDC-AED systems. The PA of TMDC-AED systems was calculated by following eq 2 using the constant value of $\Delta H_{H^+}°$ as 0.0643 eV.[33]

ASSOCIATED CONTENT

Supporting Information

The Supporting Information is available free of charge at https://pubs.acs.org/doi/10.1021/acsnano.4c02429.

> Comparison of the electro/nucleophilic site of antiepileptic drugs (AEDs) using Fukui functions; schematic of transition-state calculations of AEDs; optical spectroscopic spectra of topiramate of MoS_2; distance difference between the transition metal dichalcogenides-AEDs depending transition metal and chalcogenides variance; structure of the AEDs and their corresponding internal standards; selected mass spectra of various AEDs obtained on WTe_2 and $MoTe_2$ in positive polarity; simultaneous detection of three AEDs [carbamazepine (CBZ), lamotrigine (LTG), and topiramate (TPR)] and their corresponding internal standards; comparison between the immunoassay and the $MoTe_2$/WTe_2 mixture-assisted LDI-MS for CBZ, LTG, and TPR; Raman spectra of CVT-grown TMDCs prepared by different methods; ion signals for antiepileptic medications; and methods involved in optical spectroscopy experimental measurements (PDF)

AUTHOR INFORMATION

Corresponding Authors

Sang-Guk Lee − *Department of Laboratory Medicine, Yonsei University College of Medicine, Seoul 03722, Republic of Korea;* orcid.org/0000-0003-3862-3660; Email: comforter6@yuhs.ac

Tae Geol Lee − *Korea Research Institute of Standards and Science, Daejeon 34113, Republic of Korea;* orcid.org/0000-0002-6674-4147; Email: tglee@kriss.re.kr

Authors

Sunho Joh − *Korea Research Institute of Standards and Science, Daejeon 34113, Republic of Korea*

Jaekak Yoo − *Department of Physics, Hanyang University, Seoul 04763, Republic of Korea*

Seung Mi Lee − *Korea Research Institute of Standards and Science, Daejeon 34113, Republic of Korea;* orcid.org/0000-0002-5956-5853

Eunji Lee − *Department of Energy Science, Sungkyunkwan University, Suwon 16419, Republic of Korea*

Hee-Kyung Na − *Korea Research Institute of Standards and Science, Daejeon 34113, Republic of Korea;* orcid.org/0000-0001-9925-1149

Jin Gyeong Son − *Korea Research Institute of Standards and Science, Daejeon 34113, Republic of Korea;* orcid.org/0000-0003-2106-4014

Jeongyong Kim − *Department of Energy Science, Sungkyunkwan University, Suwon 16419, Republic of Korea;* orcid.org/0000-0003-4679-0370

Mun Seok Jeong − *Department of Physics, Hanyang University, Seoul 04763, Republic of Korea;* orcid.org/0000-0002-7019-8089

Complete contact information is available at: https://pubs.acs.org/10.1021/acsnano.4c02429

Author Contributions

⊥S.J., J.Y. contributed equally to this work.

Notes

The authors declare no competing financial interest.

ACKNOWLEDGMENTS

This work was supported by the Korea Research Institute of Standards and Science (KRISS-2024-GP2024-0007) and the Nano Material Technology Development Program (NRF-2016M3A7B6908929, NRF-2018M3D1A1058814, and 2021M3C1C3097638) of the National Research Foundation (NRF) of Korea, a National Research Council of Science & Technology (NST) grant by the Korean Government (MSIT) (no. CPS23111-110).

REFERENCES

(1) Wang, Q. H.; Kalantar-Zadeh, K.; Kis, A.; Coleman, J. N.; Strano, M. S. Electronics and optoelectronics of two-dimensional transition metal dichalcogenides. *Nat. Nanotechnol.* **2012**, *7*, 699−712.

(2) Manzeli, S.; Ovchinnikov, D.; Pasquier, D.; Yazyev, O. V.; Kis, A. 2D transition metal dichalcogenides. *Nat. Rev. Mater.* **2017**, *2*, 17033.

(3) Heine, T. Transition Metal Chalcogenides: Ultrathin Inorganic Materials with Tunable Electronic Properties. *Acc. Chem. Res.* **2015**, *48*, 65−72.

(4) Çakır, D.; Peeters, F. M.; Sevik, C. Mechanical and thermal properties of h-MX2 (M = Cr, Mo, W; X = O, S, Se, Te) monolayers: A comparative study. *Appl. Phys. Lett.* **2014**, *104*, 203110.

(5) Li, H.; Shi, Y.; Chiu, M.-H.; Li, L.-J. Emerging energy applications of two-dimensional layered transition metal dichalcogenides. *Nano Energy* **2015**, *18*, 293−305.

(6) Chimene, D.; Alge, D. L.; Gaharwar, A. K. Two-Dimensional Nanomaterials for Biomedical Applications: Emerging Trends and Future Prospects. *Adv. Mater.* **2015**, *27*, 7261−7284.

(7) Peng, B.; Ang, P. K.; Loh, K. P. Two-dimensional dichalcogenides for light-harvesting applications. *Nano Today* **2015**, *10*, 128−137.

(8) Mahler, B.; Hoepfner, V.; Liao, K.; Ozin, G. A. Colloidal Synthesis of 1T-WS2 and 2H-WS2 Nanosheets: Applications for Photocatalytic Hydrogen Evolution. *J. Am. Chem. Soc.* **2014**, *136*, 14121−14127.

(9) Kim, M.-J.; Park, J.-M.; Yun, T. G.; Noh, J.-Y.; Kang, M.-J.; Pyun, J.-C. A TiO2 nanowire photocatalyst for dual-ion production in laser desorption/ionization (LDI) mass spectrometry. *Chem. Commun.* **2020**, *56*, 4420−4423.

(10) Pei, J.; Zhao, Y.; Zhang, S.; Yu, X.; Tian, Z.; Sun, Y.; Ma, S.; Zhao, R.-S.; Meng, J.; Chen, X.; Chen, F. A Surface Matrix of Au NPs Decorated Graphdiyne for Multifunctional Laser Desorption/Ionization Mass Spectrometry. *ACS Appl. Mater. Interfaces* **2023**, *15*, 52814−52826.

(11) Kim, M.-J.; Yun, T. G.; Noh, J.-Y.; Park, J.-M.; Kang, M.-J.; Pyun, J.-C. Synergistic Effect of the Heterostructure of Au Nanoislands on TiO2 Nanowires for Efficient Ionization in Laser Desorption/Ionization Mass Spectrometry. *ACS Appl. Mater. Interfaces* **2019**, *11*, 20509−20520.

(12) Liang, W.; Yan, W.; Wang, X.; Yan, X.; Hu, Q.; Zhang, W.; Meng, H.; Yin, L.; He, Q.; Ma, C. A single atom cobalt anchored MXene bifunctional platform for rapid, label-free and high-throughput biomarker analysis and tissue imaging. *Biosens. Bioelectron.* **2024**, *246*, 115903.

(13) Yagnik, G. B.; Hansen, R. L.; Korte, A. R.; Reichert, M. D.; Vela, J.; Lee, Y. J. Large Scale Nanoparticle Screening for Small Molecule Analysis in Laser Desorption Ionization Mass Spectrometry. *Anal. Chem.* **2016**, *88*, 8926−8930.

(14) Picca, R. A.; Calvano, C. D.; Cioffi, N.; Palmisano, F. Mechanisms of Nanophase-Induced Desorption in LDI-MS. A Short Review. *Nanomaterials* **2017**, *7*, 75.

(15) Hussain, R. A.; Hussain, I. Metal telluride nanotubes: Synthesis, and applications. *Mater. Chem. Phys.* **2020**, *256*, 123691.

(16) Yin, X.; Tang, C. S.; Zheng, Y.; Gao, J.; Wu, J.; Zhang, H.; Chhowalla, M.; Chen, W.; Wee, A. T. S. Recent developments in 2D transition metal dichalcogenides: phase transition and applications of the (quasi-)metallic phases. *Chem. Soc. Rev.* **2021**, *50*, 10087−10115.

(17) Eftekhari, A. Tungsten dichalcogenides (WS2, WSe2, and WTe2): materials chemistry and applications. *J. Mater. Chem. A* **2017**, *5*, 18299−18325.

(18) Kim, Y.-K.; Wang, L.-S.; Landis, R.; Kim, C. S.; Vachet, R. W.; Rotello, V. M. A layer-by-layer assembled MoS2 thin film as an efficient platform for laser desorption/ionization mass spectrometry analysis of small molecules. *Nanoscale* **2017**, *9*, 10854−10860.

(19) Zhao, Y.; Tang, M.; Liao, Q.; Li, Z.; Li, H.; Xi, K.; Tan, L.; Zhang, M.; Xu, D.; Chen, H.-Y. Disposable MoS2-Arrayed MALDI MS Chip for High-Throughput and Rapid Quantification of Sulfonamides in Multiple Real Samples. *ACS Sens.* **2018**, *3*, 806−814.

(20) Joh, S.; Na, H.-K.; Son, J. G.; Lee, A. Y.; Ahn, C.-H.; Ji, D.-J.; Wi, J.-S.; Jeong, M. S.; Lee, S.-G.; Lee, T. G. Quantitative Analysis of Immunosuppressive Drugs Using Tungsten Disulfide Nanosheet-Assisted Laser Desorption Ionization Mass Spectrometry. *ACS Nano* **2021**, *15*, 10141−10152.

(21) Rho, J. M.; White, H. S. Brief history of anti-seizure drug development. *Epilepsia Open* **2018**, *3*, 114−119.

(22) Kawasaki, H.; Nakai, K.; Arakawa, R.; Athanassiou, E. K.; Grass, R. N.; Stark, W. J. Functionalized Graphene-Coated Cobalt Nanoparticles for Highly Efficient Surface-Assisted Laser Desorption/Ionization Mass Spectrometry Analysis. *Anal. Chem.* **2012**, *84*, 9268−9275.

(23) Luo, G.; Chen, Y.; Daniels, H.; Dubrow, R.; Vertes, A. Internal Energy Transfer in Laser Desorption/Ionization from Silicon Nanowires. *J. Phys. Chem. B* **2006**, *110*, 13381−13386.

(24) Geerlings, P.; De Proft, F.; Langenaeker, W. Conceptual Density Functional Theory. *Chem. Rev.* **2003**, *103*, 1793−1874.

(25) Yoo, J.; Yang, K.; Cho, B. W.; Kim, K. K.; Lim, S. C.; Lee, S. M.; Jeong, M. S. Identifying the Origin of Defect-Induced Raman Mode in WS2Monolayers via Density Functional Perturbation Theory. *J. Phys. Chem. C* **2022**, *126*, 4182−4187.

(26) Yoo, J.; Lee, S. M.; Lee, K.; Lim, S. C.; Jeong, M. S.; Kim, J.; Lee, T. G. Functional group inhomogeneity in graphene oxide using correlative absorption spectroscopy. *Appl. Surf. Sci.* **2023**, *613*, 155885.

(27) Yoo, J.; Cho, Y.; Jeong, B.; Choi, S. H.; Kim, K. K.; Lim, S. C.; Lee, S. M.; Choo, J.; Jeong, M. S. Explainable Artificial Intelligence Approach to Identify the Origin of Phonon-Assisted Emission in WSe2Monolayer. *Adv. Intell. Syst.* **2023**, *5*, 2200463.

(28) Philippi, F.; Rauber, D.; Springborg, M.; Hempelmann, R. Density Functional Theory Descriptors for Ionic Liquids and the Charge-Transfer Interpretation of the Haven Ratio. *J. Phys. Chem. A* **2019**, *123*, 851−861.

(29) Shi, R.; Dai, X.; Li, W.; Lu, F.; Liu, Y.; Qu, H.; Li, H.; Chen, Q.; Tian, H.; Wu, E.; et al. Hydroxyl-Group-Dominated Graphite Dots Reshape Laser Desorption/Ionization Mass Spectrometry for Small Biomolecular Analysis and Imaging. *ACS Nano* **2017**, *11*, 9500−9513.

(30) Kim, M.-J.; Noh, J.-Y.; Yun, T. G.; Kang, M.-J.; Son, D. H.; Pyun, J.-C. Laser-Shock-Driven In Situ Evolution of Atomic Defect and Piezoelectricity in Graphitic Carbon Nitride for the Ionization in Mass Spectrometry. *ACS Nano* **2022**, *16*, 18284−18297.

(31) Calais, J.-L. Density-functional theory of atoms and molecules. R.G. Parr and W. Yang, Oxford University Press, New York, Oxford, 1989. IX + 333 pp. Price £45.00. *Int. J. Quantum Chem.* **1993**, *47*, 101.

(32) Asakawa, D.; Takahashi, H.; Iwamoto, S.; Tanaka, K. Fundamental study of hydrogen-attachment-induced peptide fragmentation occurring in the gas phase and during the matrix-assisted laser desorption/ionization process. *Phys. Chem. Chem. Phys.* **2018**, *20*, 13057−13067.

(33) Grechnikov, A. A.; Borodkov, A. S.; Alimpiev, S. S.; Nikiforov, S. M.; Simanovsky, Y. O. Gas-phase basicity: Parameter determining

https://doi.org/10.1021/acsnano.4c02429

the efficiency of laser desorption/ionization from silicon surfaces. *J. Anal. Chem.* **2013**, *68*, 19−26.

(34) Brancia, F. L.; Stener, M.; Magistrato, A. A density functional theory (DFT) study on gas-phase proton transfer reactions of derivatized and underivatized peptide ions generated by matrix-assisted laser desorption ionization. *J. Am. Soc. Mass Spectrom.* **2009**, *20*, 1327−1333.

(35) Alimpiev, S.; Grechnikov, A.; Sunner, J.; Borodkov, A.; Karavanskii, V.; Simanovsky, Y.; Nikiforov, S. Gas Chromatography/Surface-Assisted Laser Desorption Ionization Mass Spectrometry of Amphetamine-like Compounds. *Anal. Chem.* **2009**, *81*, 1255−1261.

(36) Alimpiev, S.; Grechnikov, A.; Sunner, J.; Karavanskii, V.; Simanovsky, Y.; Zhabin, S.; Nikiforov, S. On the role of defects and surface chemistry for surface-assisted laser desorption ionization from silicon. *J. Chem. Phys.* **2008**, *128*, 014711.

(37) Chen, Y.; Chen, H.; Aleksandrov, A.; Orlando, T. M. Roles of water, acidity and surface morphology in surface-assisted laser desorption/ionization of amino acids. *J. Phys. Chem. C* **2008**, *112*, 6953−6960.

(38) Silina, Y. E.; Koch, M.; Volmer, D. A. The role of physical and chemical properties of Pd nanostructured materials immobilized on inorganic carriers on ion formation in atmospheric pressure laser desorption/ionization mass spectrometry. *J. Mass Spectrom.* **2014**, *49*, 468−480.

(39) Xiao, Y.; Retterer, S. T.; Thomas, D. K.; Tao, J.-Y.; He, L. Impacts of Surface Morphology on Ion Desorption and Ionization in Desorption Ionization on Porous Silicon (DIOS) Mass Spectrometry. *J. Phys. Chem. C* **2009**, *113*, 3076−3083.

(40) Silina, Y. E.; Volmer, D. a. Nanostructured solid substrates for efficient laser desorption/ionization mass spectrometry (LDI-MS) of low molecular weight compounds. *Analyst* **2013**, *138*, 7053−7065.

(41) Stolee, J. A.; Walker, B. N.; Zorba, V.; Russo, R. E.; Vertes, A. Laser−nanostructure interactions for ion production. *Phys. Chem. Chem. Phys.* **2012**, *14*, 8453−8471.

(42) Luo, G.; Chen, Y.; Daniels, H.; Dubrow, R.; Vertes, A. Internal energy transfer in laser desorption/ionization from silicon nanowires. *J. Phys. Chem. B* **2006**, *110*, 13381−13386.

(43) Ding, Y.; Pei, C.; Li, K.; Shu, W.; Hu, W.; Li, R.; Zeng, Y.; Wan, J. Construction of a ternary component chip with enhanced desorption efficiency for laser desorption/ionization mass spectrometry based metabolic fingerprinting. *Front. Bioeng. Biotechnol.* **2023**, *11*, 1118911.

(44) Zhu, Y.; Wang, J.; Zeng, P.; Fu, C.; Chen, D.; Jiang, Y.; Sun, Y.; Xie, Z. Novel Ag-modified vanadate nanosheets for determination of small organic molecules with laser desorption ionization mass spectrometry. *J. Hazard. Mater.* **2024**, *464*, 132986.

(45) Cheng, Y.-H.; Ng, K.-M. The Hidden Heroes: Holes in Charge-Driven Desorption Mass Spectrometry. *Anal. Chem.* **2020**, *92*, 5645−5649.

(46) Cheng, Y.-H.; Ng, K.-M. Sensitive Detection of Separated Charges in Nanohybrids by Laser Excitation Mass Spectrometry with Tetrabutylammonium Cationic Probe. *Anal. Chem.* **2020**, *92*, 10262−10267.

(47) Zulfiqar, M.; Zhao, Y.; Li, G.; Li, Z.; Ni, J. Intrinsic Thermal conductivities of monolayer transition metal dichalcogenides MX2 (M = Mo, W; X = S, Se, Te). *Sci. Rep.* **2019**, *9*, 4571.

(48) Zhang, Z.; Xie, Y.; Ouyang, Y.; Chen, Y. A systematic investigation of thermal conductivities of transition metal dichalcogenides. *Int. J. Heat Mass Transfer* **2017**, *108*, 417−422.

(49) Lee, B. I.; Park, K. M.; Kim, S. E.; Heo, K. Clinical opinion: Earlier employment of polytherapy in sequential pharmacotherapy of epilepsy. *Epilepsy Res.* **2019**, *156*, 106165.

(50) Willems, L. M.; Hamer, H. M.; Knake, S.; Rosenow, F.; Reese, J.-P.; Strzelczyk, A. General Trends in Prices and Prescription Patterns of Anticonvulsants in Germany between 2000 and 2017: Analysis of National and Cohort-Based Data. *Appl. Health Econ. Health Pol.* **2019**, *17*, 707−722.

(51) Kang, K. W.; Lee, H.; Shin, J.-Y.; Moon, H.-J.; Lee, S.-Y. Trends in Prescribing of Antiseizure Medications in South Korea: Real-World Evidence for Treated Patients With Epilepsy. *J. Clin. Neurol.* **2022**, *18*, 179−193.

(52) Wang, D.; Baudys, J.; Krilich, J.; Smith, T. J.; Barr, J. R.; Kalb, S. R. A Two-Stage Multiplex Method for Quantitative Analysis of Botulinum Neurotoxins Type A, B, E, and F by MALDI-TOF Mass Spectrometry. *Anal. Chem.* **2014**, *86*, 10847−10854.

(53) Gao, J.; Meyer, K.; Borucki, K.; Ueland, P. M. Multiplex Immuno-MALDI-TOF MS for Targeted Quantification of Protein Biomarkers and Their Proteoforms Related to Inflammation and Renal Dysfunction. *Anal. Chem.* **2018**, *90*, 3366−3373.

(54) Xu, H.; Liu, M.; Huang, X.; Min, Q.; Zhu, J.-J. Multiplexed Quantitative MALDI MS Approach for Assessing Activity and Inhibition of Protein Kinases Based on Postenrichment Dephosphorylation of Phosphopeptides by Metal−Organic Framework-Templated Porous CeO2. *Anal. Chem.* **2018**, *90*, 9859−9867.

(55) Taraskin, A. S.; Semenov, K. K.; Lozhkov, A. A.; Baranovskaya, I. L.; Protasov, A. V.; Ramsay, E. S.; Tyulin, A. A.; Mirgorodskaya, O. A.; Vasin, A. V.; Klotchenko, S. A.; Zabrodskaya, Y. A. A novel method for multiplex protein biomarker analysis of human serum using quantitative MALDI mass spectrometry. *J. Pharm. Biomed. Anal.* **2022**, *210*, 114575.

(56) Aouri, M.; Moradpour, D.; Cavassini, M.; Mercier, T.; Buclin, T.; Csajka, C.; Telenti, A.; Rauch, A.; Decosterd, L. A. Multiplex Liquid Chromatography-Tandem Mass Spectrometry Assay for Simultaneous Therapeutic Drug Monitoring of Ribavirin, Boceprevir, and Telaprevir. *Antimicrob. Agents Chemother.* **2013**, *57*, 3147−3158.

(57) Li, C.; Ye, Z.; Xu, Y.; Bell, S. E. J. An overview of therapeutic anticancer drug monitoring based on surface enhanced (resonance) Raman spectroscopy (SE(R)RS). *Analyst* **2020**, *145*, 6211−6221.

(58) Ates, H. C.; Mohsenin, H.; Wenzel, C.; Glatz, R. T.; Wagner, H. J.; Bruch, R.; Hoefflin, N.; Spassov, S.; Streicher, L.; Lozano-Zahonero, S.; et al. Biosensor-Enabled Multiplexed On-Site Therapeutic Drug Monitoring of Antibiotics. *Adv. Mater.* **2022**, *34*, 2104555.

(59) Krasowski, M. D.; Long, T. A.; Snozek, C. L. H.; Dizon, A.; Magnani, B.; Melanson, S. E. F. Therapeutic drug monitoring of second- and third-generation antiepileptic drugs. *Arch. Pathol. Lab Med.* **2021**, *145*, 1485−1491.

(60) Krasowski, M. D.; McMillin, G. A. Advances in anti-epileptic drug testing. *Clin. Chim. Acta* **2014**, *436*, 224−236.

(61) Opuni, K. F. M.; Boadu, J. A.; Amponsah, S. K.; Okai, C. A. High performance liquid chromatography: A versatile tool for assaying antiepileptic drugs in biological matrices. *J. Chromatogr. B: Anal. Technol. Biomed. Life Sci.* **2021**, *1179*, 122750.

(62) Kang, J.; Park, Y.-S.; Kim, S.-H.; Kim, S.-H.; Jun, M.-Y. Modern methods for analysis of antiepileptic drugs in the biological fluids for pharmacokinetics, bioequivalence and therapeutic drug monitoring. *Korean J. Physiol. Pharmacol.* **2011**, *15*, 67−81.

(63) Sommerfeld-Klatta, K.; Zielińska-Psuja, B.; Karaźniewcz-Łada, M.; Główka, F. K. New methods used in pharmacokinetics and therapeutic monitoring of the first and newer generations of antiepileptic drugs (AEDs). *Molecules* **2020**, *25*, 5083.

(64) Kong, S. T.; Lim, S.-H.; Lee, W. B.; Kumar, P. K.; Wang, H. Y. S.; Ng, Y. L. S.; Wong, P. S.; Ho, P. C. Clinical Validation and Implications of Dried Blood Spot Sampling of Carbamazepine, Valproic Acid and Phenytoin in Patients with Epilepsy. *PLoS One* **2014**, *9*, No. e108190.

(65) Kuchekar, S. R.; Kundlik, M. L.; Zaware, B. H. Rapid and specific approach for direct measurement of topiramate in human plasma by LC-MS/MS: Application for bioequivalence study. *J. Bioanal. Biomed.* **2010**, *02*, 107−112.

(66) Delley, B. An all-electron numerical method for solving the local density functional for polyatomic molecules. *J. Chem. Phys.* **1990**, *92*, 508−517.

(67) Stephens, P. J.; Devlin, F. J.; Chabalowski, C. F.; Frisch, M. J. Ab Initio Calculation of Vibrational Absorption and Circular Dichroism Spectra Using Density Functional Force Fields. *J. Phys. Chem.* **1994**, *98*, 11623−11627.

(68) Fukui, K.; Yonezawa, T.; Shingu, H. A Molecular Orbital Theory of Reactivity in Aromatic Hydrocarbons. *J. Chem. Phys.* **1952**, *20*, 722−725.

(69) Parr, R. G.; Yang, W. Density functional approach to the frontier-electron theory of chemical reactivity. *J. Am. Chem. Soc.* **1984**, *106*, 4049−4050.

(70) Halgren, T. A.; Lipscomb, W. N. The synchronous-transit method for determining reaction pathways and locating molecular transition states. *Chem. Phys. Lett.* **1977**, *49*, 225−232.

(71) Perdew, J. P.; Burke, K.; Ernzerhof, M. Generalized Gradient Approximation Made Simple. *Phys. Rev. Lett.* **1996**, *77*, 3865−3868.

(72) Rasmussen, F. A.; Thygesen, K. S. Computational 2D Materials Database: Electronic Structure of Transition-Metal Dichalcogenides and Oxides. *J. Phys. Chem. C* **2015**, *119*, 13169−13183.

(73) Huang, W.; Da, H.; Liang, G. Thermoelectric performance of MX2 (M = Mo,W; X = S,Se) monolayers. *J. Appl. Phys.* **2013**, *113*, 104304.

(74) Mortazavi, B.; Berdiyorov, G. R.; Makaremi, M.; Rabczuk, T. Mechanical responses of two-dimensional MoTe2; pristine 2H, 1T and 1T′ and 1T′/2H heterostructure. *Extreme Mech. Lett.* **2018**, *20*, 65−72.

(75) Zheng, F.; Cai, C.; Ge, S.; Zhang, X.; Liu, X.; Lu, H.; Zhang, Y.; Qiu, J.; Taniguchi, T.; Watanabe, K.; Jia, S.; Qi, J.; Chen, J.-H.; Sun, D.; Feng, J. On the Quantum Spin Hall Gap of Monolayer 1T′-WTe2. *Adv. Mater.* **2016**, *28*, 4845−4851.

https://doi.org/10.1021/acsnano.4c02429